

CNS-restricted Transduction and CRISPR/Cas9-mediated Gene Deletion with an Engineered AAV Vector

Giridhar Murlidharan^{1,2}, Kensuke Sakamoto³, Lavanya Rao¹, Travis Corriher¹, Dan Wang⁴, Guangping Gao⁴, Patrick Sullivan³ and Aravind Asokan^{1,3,5}

Gene therapy using recombinant adeno-associated viral (AAV) vectors is emerging as a promising approach to treat central nervous system disorders such as Spinal muscular atrophy, Batten, Parkinson and Alzheimer disease amongst others. A critical remaining challenge for central nervous system-targeted gene therapy, silencing or gene editing is to limit potential vector dose-related toxicity in off-target cells and organs. Here, we characterize a lab-derived AAV chimeric (AAV2g9), which displays favorable central nervous system attributes derived from both parental counterparts, AAV2 and AAV9. This synthetic AAV strain displays preferential, robust, and widespread neuronal transduction within the brain and decreased glial tropism. Importantly, we observed minimal systemic leakage, decreased sequestration and gene transfer in off-target organs with AAV2g9, when administered into the cerebrospinal fluid. A single intracranial injection of AAV2g9 vectors encoding guide RNAs targeting the schizophrenia risk gene MIR137 (encoding MIR137) in CRISPR/Cas9 knockin mice resulted in brain-specific gene deletion with no detectable events in the liver. This engineered AAV vector is a promising platform for treating neurological disorders through gene therapy, silencing or editing modalities.

Molecular Therapy—Nucleic Acids (2016) 5, e338; doi:10.1038/mtna.2016.49; published online 19 July 2016

Subject Category: gene addition, deletion and modification gene vectors

Introduction

Recombinant adeno-associated viral (AAV) vectors have met safety endpoints in several phase 1 gene therapy clinical trials for treating Hemophilia, Alpha-1 Antitrypsin deficiency, and Alzheimer disease amongst other indications.^{1–3} Although vector redosing might be essential in some indications due to loss of gene expression observed in long term follow up studies,⁴ preclinical studies continue to show promise and advance with cautious optimism. One concern noted in hemophilia gene therapy clinical trials is the potential for vector dose-related hepatotoxicity in patients as evidenced by a rise in transaminases.^{2,5} Although resolvable by administration of anti-inflammatory steroids such as methyl prednisolone, permanent loss in gene expression has been observed.² The dose and composition of clinical AAV vectors has been shown to influence these outcomes in preclinical toxicity studies.⁶

Concurrent with the advent of AAV vector technology, recent studies in animal models have demonstrated the application of clustered, regularly interspaced, short palindromic repeats (CRISPR)/Cas9 technology for targeted disruption of genomic loci *in vivo*,^{7–10} as well as disease correction.^{8,11,12} While the recombinant AAV vector platform offers a versatile platform for therapeutic delivery of CRISPR/Cas9 *in vivo*, integration of the two technologies can pose unique challenges to clinical translation.

So far, over a hundred naturally occurring strains of AAV derived from human and animal tissues have been

isolated.^{13,14} Multiple strains ranging from AAV serotypes 1–9 and Rh.10 are under active development as gene therapy vectors for different clinical indications.^{15,16} Recent data from clinical gene therapy trials to treat Parkinson and Alzheimer disease have provided information that is critical toward continued AAV vector development.^{3,17} In addition, preclinical studies involving intravascular/intrathecal (IT) administration in mouse, canine, feline, and nonhuman primate models have supported the advancement of serotypes such as AAV9 as candidates for clinical trials.^{18–22} Notably, AAV9 is currently being evaluated in phase 1 clinical trials for the treatment of Spinal muscular atrophy by intravascular injection and Giant axonal neuropathy through IT injection (Clinical trial identifiers NCT02122952 and NCT02362438).

A key observation from preclinical studies is that central nervous system (CNS) administration of several naturally occurring AAV strains often results in vector sequestration within peripheral organs such as the liver and spleen via systemic leakage.^{19,22–24} In this study, we address this potential concern through vector design. We have previously demonstrated grafting of the galactose binding motif from AAV9 capsid, onto other AAV surfaces as a viable strategy to engineer AAV vectors with novel gene transfer properties. Specifically, the viral protein 3 amino acid residues on AAV9 capsid required for galactose binding were used to replace corresponding residues on the AAV2 capsid (viral protein1 numbering: Q464V, A467P, D469N, I470M, R471A, D472V, S474G, Y500F, S501A) using site-directed mutagenesis.

¹Gene Therapy Center, University of North Carolina at Chapel Hill, Chapel Hill, North Carolina, USA; ²Curriculum in Genetics & Molecular Biology, University of North Carolina at Chapel Hill, Chapel Hill, North Carolina, USA; ³Department of Genetics, University of North Carolina at Chapel Hill, Chapel Hill, North Carolina, USA; ⁴Gene Therapy Center, University of Massachusetts Medical School, Worcester, Massachusetts, USA; ⁵Department of Biochemistry & Biophysics, University of North Carolina at Chapel Hill, Chapel Hill, North Carolina, USA. Correspondence: Aravind Asokan, CB # 7352, Gene Therapy Center, 5123 Thurston Building, The University of North Carolina at Chapel Hill, Chapel Hill, North Carolina 27599-7352, USA. E-mail: aravind@med.unc.edu

Received 21 April 2016; accepted 25 May 2016; published online 19 July 2016. doi:10.1038/mtna.2016.49

This resulted in rational engineering of a chimeric AAV strain (AAV2g9) which harbors the ability to engage either heparan sulfate (HS) or galactose as receptors for cell entry.^{25,26} Earlier studies employing a similar approach were used to replace the HS binding motif of AAV2 (585-RGNRQA-590) with the corresponding residues of AAV8 (585-QQNTAP-590). This resulted in the engineering of HS binding deficient version of AAV2 capsid *i.e.*, AAV2i8. The latter heparin-binding deficient capsid was then used as a template toward the generation of chimeric AAV2i8g9 (ref. 37). In this study, we demonstrate exceptional CNS transduction efficiency following single bolus injections of AAV2g9 as validated by two routes of administration in neonatal and adult rodents. More importantly, we establish potentially useful attributes of AAV2g9 for CNS-specific gene therapy applications, namely, preferential neuronal tropism, restricted CNS biodistribution and minimal transgene expression in off-target peripheral organs. Furthermore, we extend these findings to demonstrate the utility of AAV2g9 for targeted disruption of the MIR137 locus in CRISPR/Cas9 transgenic mouse.⁹

Results

AAV2g9 and AAV9 display similar spread and transduction efficiencies in the CNS

We first carried out neonatal (P0) mouse intracerebroventricular injections (ICV) comparing AAV2g9 and AAV9 vectors packaging a self-complementary green fluorescent protein (ScGFP) cassette driven by the ubiquitous chicken β actin hybrid (CBh) promoter. At 2 weeks post administration (3.5×10^9 vector genomes (vg)/mouse), diaminobenzidine immunohistochemistry and confocal microscopy analysis of postfixed mouse brain sections revealed extensive GFP expression across multiple sections in the rostrocaudal axis of the mouse brain for both AAV strains (Figure 1a). Specifically, we observed robust transduction in the olfactory bulb, striatum, hippocampus, and cortical regions of the mouse brain. High magnification insets further demonstrate that AAV9 injections result in GFP expression in cells with neuronal or glial morphology. On the other hand, mice injected with AAV2g9 show selective GFP expression in neurons. Furthermore, it is important to note that AAV2g9 injections result in robust GFP expression in the CNS tissue immediately surrounding lateral ventricular cerebrospinal fluid (CSF) space. Specifically, we observed strong transduction along the hippocampal boundary within the caudal sections of AAV2g9 injected mouse brains. On a cellular level, these are mixture of ependymal cells and neuronal projections within corpus callosum and medial forebrain bundle system. This robust transduction was not observed due to AAV9 administrations.

To further compare cellular transduction profiles of the two vectors, we generated higher magnification confocal micrographs of functionally relevant regions of the brain including the cortex, amygdala, hypothalamus, and hippocampus. Mice injected with AAV9 or AAV2g9 showed comparably robust GFP expression in these regions (Figure 1b). Additionally, we observed that while AAV9 treatment resulted in GFP+ cells with neuronal or glial morphology, AAV2g9 mediated GFP expression was mostly restricted to neurons. We further validated this observation using immune colocalization with

the neuronal antigen marker, NeuN or glial fibrillary acid protein marker, glial fibrillary acid protein (GFAP). These results were further confirmed upon quantitation, which revealed a ~4 fold reduction in GFP+ cells with glial morphology for AAV2g9, but no significant differences between the two vectors in neuronal populations (Figure 3a,b). Overall, these results suggest that AAV2g9 spreads efficiently across the neonatal mouse brain, while demonstrating a robust and neurotropic transduction profile from a single unilateral ICV injection.

AAV2g9 and AAV9 display different cell-type specificities in the CNS

We then generated AAV9 and AAV2g9 vectors packaging single-stranded (ss) GFP cassettes driven by the neuron-specific human synapsin I (hSyn) or the glia-specific GFAP promoter. Vectors (3.5×10^9 vg/mouse) were administered in postnatal day 0 (P0) mice via the ICV route and postfixed brain tissues analyzed at 2 weeks postadministration by diaminobenzidine immunohistochemistry, immunostaining, and confocal microscopy analysis. Both AAV9 and AAV2g9 vectors packaging transgene driven by hSyn promoter displayed robust transduction across multiple sections of the mouse brain (Figure 2a). Specifically, we observed GFP+ cells colocalizing with NeuN+ cells (yellow) in various regions including the striatum, cortex, hippocampus, amygdala, and hypothalamus (Figure 2b). As expected, no glial staining was observed for either vector supporting the potential application of such neuron-specific promoters for CNS gene therapy studies.

In contrast, to hSyn promoter driven expression, we observed striking differences in the patterns of GFP expression mediated by AAV9 and AAV2g9 vectors packaging the GFAP promoter driven transgene cassette. Notably, AAV9 injections resulted in widespread GFP expression in cells with glial morphology across the entire brain parenchyma in multiple brain sections (Figure 2c). In contrast, mice injected with AAV2g9 exhibit spatially restricted GFP expression within close proximity of the site of CSF injection (lateral ventricles) or along the immediate point of contact between the CSF and brain parenchyma, the inner meninges. To further confirm these observations, we coimmunostained different sections of the mouse brain for GFP expression (green) with neuronal marker-NeuN or glial marker-GFAP (red) as before. High magnification confocal micrographs generated at different brain regions show robust GFP+ expression from AAV9 injections in GFAP+ cells, but not NeuN+ cells (Figure 2d). These observed patterns of transgene expression were further confirmed by quantitative analysis, which revealed ~2.5-fold reduction in glial transduced area throughout the brain with AAV2g9 vectors under GFAP promoter activity (Figure 3c,d). These results demonstrate that AAV9 vectors packaging GFAP promoter driven expression cassettes are excellent candidates for glial gene transfer applications, while AAV2g9 appears to more neurotropic and hence suitable for CNS gene transfer applications targeting neuronal populations. From the AAV biology perspective, AAV2g9 appears to preferentially transduce neurons over glia, while this is patently not the case with AAV9.

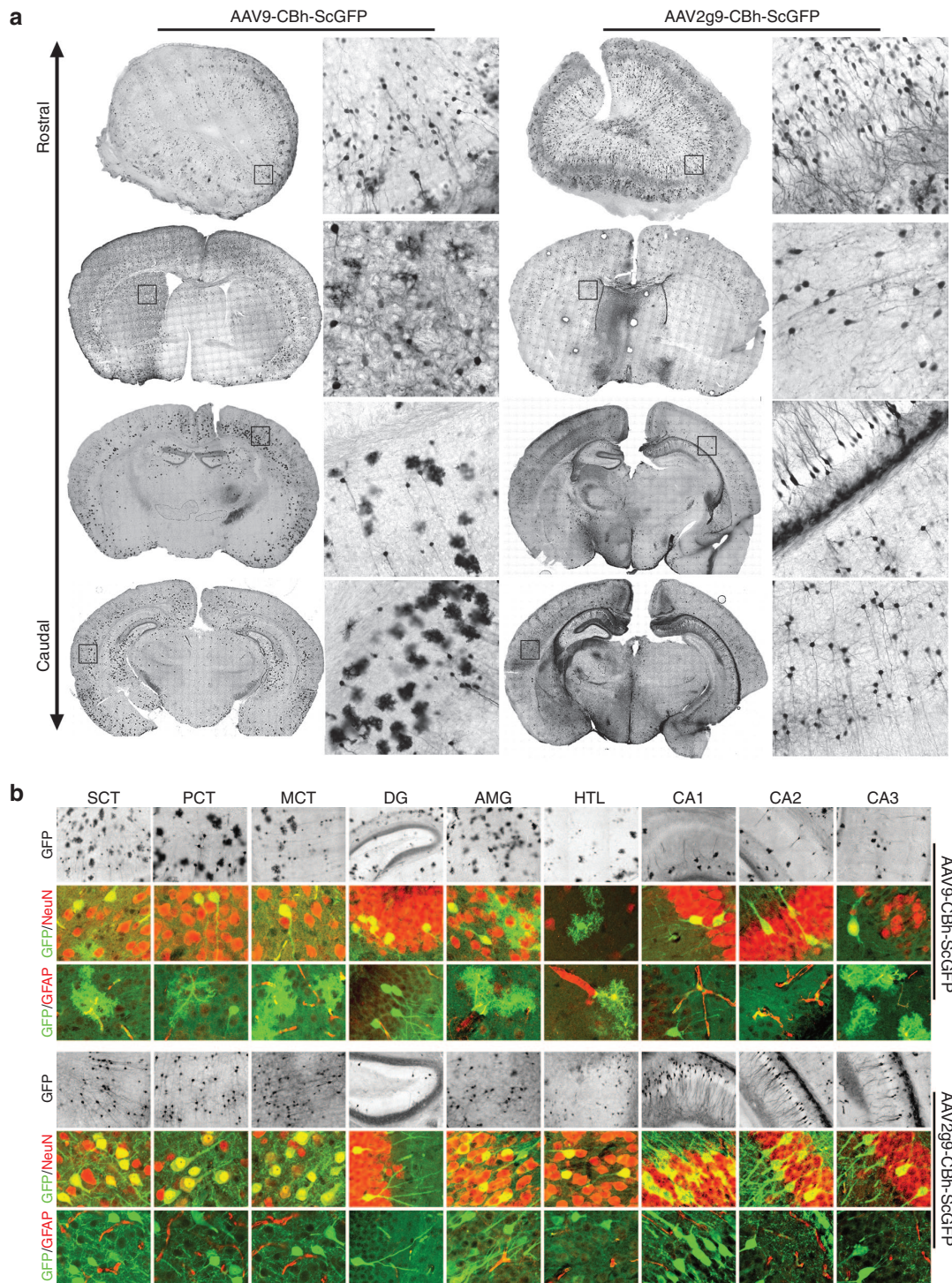


Figure 1 Comparison of transgene (GFP) expression and cellular tropisms displayed by AAV9 and AAV2g9 vectors with a ubiquitous promoter after ventricular (ICV) injection. Postnatal day 0 (P0) mice were injected with equal viral titers (3.5×10^9 vg) of AAV9 or AAV2g9 packaging a ScGFP transgene driven by a ubiquitous chicken β hybrid (CBh) promoter into the left lateral ventricle. At 2 weeks post vector administration, the mice were sacrificed and paraformaldehyde postfixed brains were sectioned and immunostained as described earlier. **(a)** Representative images of coronal sections obtained from olfactory bulbs, lateral ventricles and hippocampi are shown. Inset images from whole brain sections are shown to the right of each section at higher magnification. **(b)** Top image panel shows higher magnification images of DAB staining (GFP expression) in functionally relevant regions of the mouse brain namely; somatosensory cortex (SCT), piriform (PCT), motor CT (MCT), dentate gyrus (DG), amygdala (AMG), hypothalamus (HTL) and hippocampal CA1, CA2 and CA3 are shown. Middle and bottom panels show immuno-colocalization of GFP expression (green) with neuronal marker, NeuN or glial marker, GFAP (red). All experiments were conducted in triplicate and representative images are shown. GFAP, glial fibrillary acid protein; DAB, diaminobenzidine; GFP, green fluorescent protein; ICV, intracerebroventricular injections.

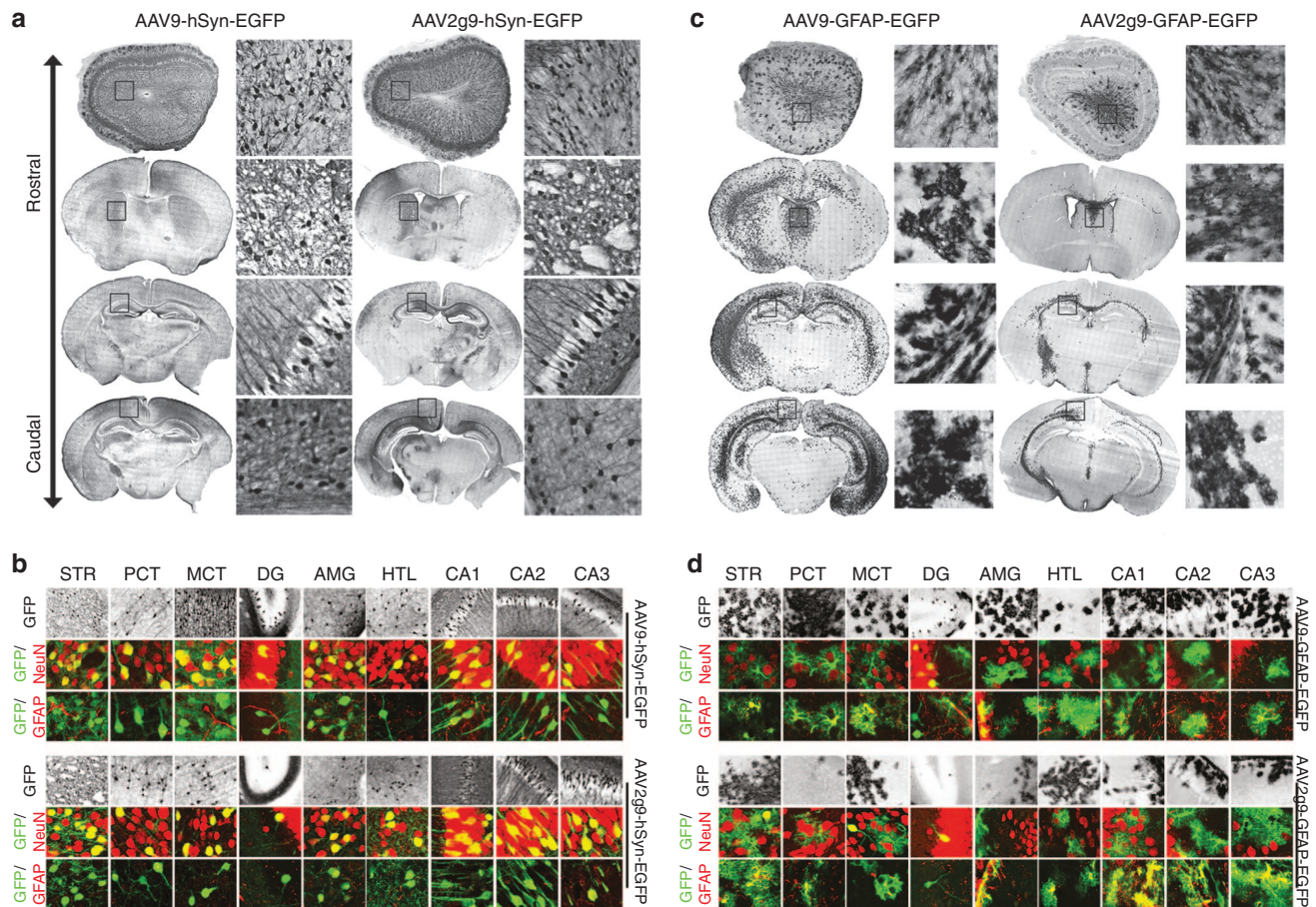


Figure 2 Comparison of transgene (GFP) expression and cellular tropisms displayed by AAV9 and AAV2g9 vectors with cell type-specific promoters after ventricular (ICV) injection. Postnatal day 0 (P0) mice were injected with equal viral titers (3.5×10^9 vg) of AAV9 or AAV2g9 packaging a single-stranded GFP (ssGFP) transgene driven by the **a,b** hSyn promoter or the **c,d** GFAP promoter into the left lateral ventricle. At 2 weeks post vector administration, the mice were sacrificed and paraformaldehyde postfixed brains were sectioned and immunostained. Diaminobenzidine (DAB) immunohistochemistry was used to detect GFP expression. (**a,c**) Representative images of coronal sections obtained from olfactory bulbs, lateral ventricles, and hippocampi are shown. Inset images from whole brain sections are shown to the right of each section at higher magnification. (**b,d**) Representative confocal images of coronal tissue sections at higher magnification. Top image panel shows higher magnification images of DAB staining (GFP expression) in functionally relevant regions of the mouse brain namely; Striatum (STR), piriform CT, Motor CT, dentate gyrus (DG), amygdala (AMG), hypothalamus (HTL) and hippocampal CA1, CA2 and CA3 regions are shown. Middle and bottom panels show immuno-colocalization of GFP expression (green) with neuronal marker, NeuN or glial marker, GFAP (red) obtained using a Zeiss CLSM 700 confocal laser scanning microscope equipped with 488, 555, and 647nm excitation filters. Colocalized cells are pseudocolored yellow (GFP/NeuN or GFP/GFAP overlay). All experiments were conducted in triplicate and representative images are shown. AAV, adeno-associated viral; GFAP, glial fibrillary acid protein; GFP, green fluorescent protein; ICV, intracerebroventricular injections.

HS is critical for preferential neuronal transduction by AAV2g9 vectors

The interaction of AAV2 vectors with HS proteoglycans is associated with preferential neuronal transduction in the immediate vicinity to site of CNS administration.^{27,28} Co-administration of soluble heparin has been shown to block the ability of AAV2 to bind hep and alter transduction profiles *in vitro* and *in vivo*.^{29–31} Therefore, we compared the CNS transduction profiles of AAV2 and AAV2g9 to coinjections of AAV2g9 with 1 μ g of soluble heparin in the neonatal mouse brain. Further, we generated a hep binding mutant, AAV2i8g9, as described in earlier studies by our lab.²⁶ Specifically, we injected equal viral titers (3.5×10^9 vg) of AAV2, AAV2g9, and AAV2g9 + soluble heparin or AAV2i8g9 packaging CBh-ScGFP transgene via the ICV route in P0 mice.

As shown in **Figure 4a**, we observed a low level of GFP+ expression as evidenced by diaminobenzidine immunostaining within the hippocampal sections of AAV2 injected mouse brains. Consistent with earlier results, AAV2g9 displayed robust and widespread CNS transgene expression supporting the notion that the gal footprint enhances transduction efficiency and spread. Further, we observed a decrease in GFP+ expression across the brain parenchyma in AAV2g9 + soluble heparin treated animals as well as AAV2i8g9 treated mouse cohorts in comparison with AAV2g9 (**Figure 4b–d**).

High magnification confocal micrographs of multiple regions of the mouse brain, namely; the somatosensory cortex, piriform cortex, motor cortex, dentate gyrus, amygdala, and hippocampal CA1, CA2, and CA3 regions were then generated. As seen in the top panel of **Figure 4e**, we

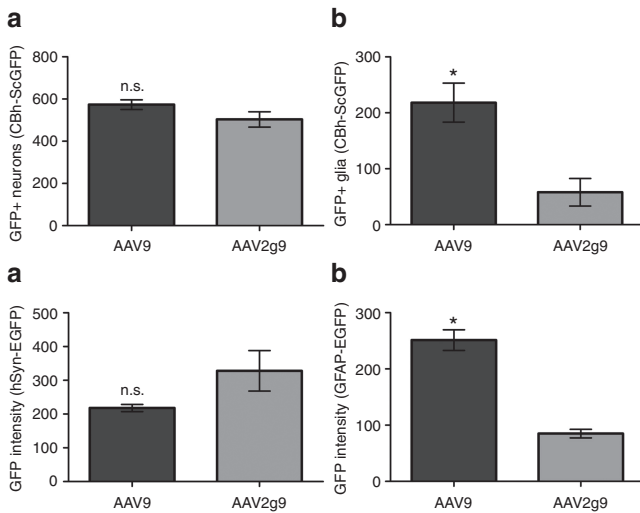


Figure 3 Quantitative assessment of transduction following ICV administration of AAV9 and AAV2g9 vectors. GFP expression was quantified in representative hippocampal sections of the mouse brains treated with AAV9 or AAV2g9 vectors. Specifically, GFP+ cells with neuronal (a) or glial (b) morphology were counted in different cortical regions including the retrosplenial, posterior parietal, somatosensory, auditory, and piriform areas. Further, quantitative assessment of GFP expression following ICV administration of AAV9 and AAV2g9 vectors driven by (c) human synapsin (hSyn) promoter or (d) glial fibrillary acid protein (GFAP) promoter was carried out using ImageJ analysis software. Specifically, the mean intensity calculator function was applied across multiple sections of the mouse brain including sections of the olfactory bulbs, lateral ventricles and hippocampal regions. Data is represented as mean \pm SD, * represents $P < 0.05$ and n.s. indicates not statistically significant ($P > 0.05$) as determined by student's *t*-test. All experiments were conducted in quadruplicate. AAV, adeno-associated viral; GFP, green fluorescent protein; ICV, intracerebroventricular injections.

observed sporadic expression in neurons and astrocytes in case of AAV2-injected mice. On the other hand, extensive and preferential neuronal transduction was observed across these regions in case of AAV2g9 as observed earlier (Figure 4e, second row panel). In contrast, loss of hep binding, either by competitive inhibition with soluble heparin or with the AAV2i8g9 mutant resulted in a decreased neuronal transduction in multiple brain regions (third row and bottom row panels, Figure 4e). In addition, loss of neuronal transduction was accompanied by an increase in GFP+ cells with glial (astrocytic) morphology in these cohorts. Taken together, our observations suggest that hep binding is critical in determining the preferential neuronal tropism displayed by AAV2g9.

AAV2g9 and AAV9 display similar transduction profiles in adult mice after IT administration

To compare the two strains in adult mice, we carried out IT infusions of AAV9 or AAV2g9 packaging CBh-ScGFP reporter transgene into the lumbar CSF space of 8 week old mice. At 3 weeks postadministration of 1×10^{11} vg/mouse, we subjected postfixed tissues to immunohistochemical analyses and confocal imaging as outlined in online methods. As shown in Figure 5a, IT infusions of both AAV9 and AAV2g9 resulted in strong transgene expression in the lumbar, thoracic, and cervical spinal cord regions. Of note, we observed GFP expression in multiple gray and white matter regions of

the spinal cord. Further, we compared cellular transduction profiles resulting from IT infusions of AAV9/2g9 vectors. Specifically, we focused on different regions of the adult CNS, namely: ventral horn, dorsal horn, intermediate gray matter region, ventral funiculus, lateral funiculus, ventral commissure, and rubrospinal tract. As shown in Figure 5b, both AAV2g9 and AAV9 infused mice exhibit robust GFP expression in these regions of the spinal cord. In both AAV9 and AAV2g9 injected mice, we observed that the GFP+ cells (green) in the gray matter regions of the spinal cord (ventral horn, dorsal horn, and intermediate) extensively colocalized with NeuN+ as well as GFAP+ cells. Within the white matter regions of spinal cord (ventral funiculus, lateral funiculus, ventral commissure, and rubrospinal tract), the GFP+ (green) cells from either injection extensively colocalized with GFAP+ cells (Figure 5b). In addition, we observe a consistent drop in transduction in progressive rostral sections of the brain from IT administrations of AAV9 or AAV2g9 (data not shown). It is important to note that parameters such as vector dose, volume, and infusion rates will likely need to be optimized further to achieve widespread gene transfer in the brain following IT injections. Overall, these observations also underscore the influence of route of injection on the cellular tropism of different AAV vectors.

AAV2g9 and AAV9 display distinct systemic biodistribution and off-target transduction profiles following CNS administration

Having established the robustness of the rationally engineered AAV2g9 strain, we compared the systemic leakage, vg biodistribution and gene expression profiles in peripheral organs resulting from ICV or IT injections of AAV9 and AAV2g9 in both neonatal and adult mice. At 3 days postadministration, we extracted whole genomic DNA from different organs and determined vg copies using quantitative polymerase chain reaction (PCR) in different peripheral organs including the liver, heart, and spleen. We observed a striking difference between the off-target biodistribution profiles of AAV9 and AAV2g9 vectors following ICV or IT injections. As seen in Figure 6a–c, in the AAV9 injected neonatal mouse cohort, ~40, 30, and 3% of the viral genomes were recovered from the liver, heart, and spleen, respectively, in comparison with the brain (normalized to 100%). In contrast, AAV2g9 vg copy numbers ranged from ~1.4, 0.7, and 0.003% in these peripheral organs. In the adult mouse cohort, AAV9 vg copies recovered in the liver, heart, and spleen were 188, 81, and 59%, respectively in comparison with vg copies recovered from the spinal cord (normalized to 100%). In contrast, only ~3, 4.5, and 10% of vg copies were recovered from these systemic organs in the AAV2g9-treated cohort (Figure 6e–g). These results suggest that unlike AAV9, AAV2g9 is sparingly sequestered in off-target, systemic organs following CNS administration.

To further corroborate the biodistribution results, we harvested different peripheral organs from the ICV and IT mouse cohorts treated with either AAV2g9 or AAV9 and subjected postfixed tissue to immunostaining and confocal imaging analysis as outlined earlier. We observed robust GFP expression in the heart, liver, and spleen of both neonatal (ICV) (Figure 6d) and adult (IT) (Figure 6h) mice treated

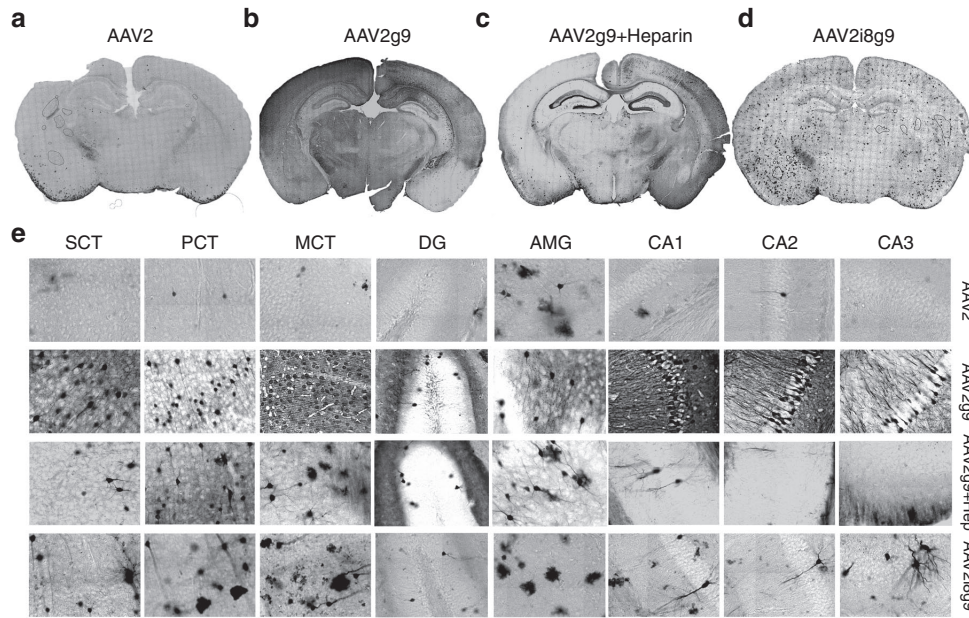


Figure 4 Heparan sulfate (HS) interactions are critical toward preferential neuronal transduction by AAV2g9 vectors. Postnatal day 0 (P0) mice were injected with equal viral titers (3.5×10^9 vg) of AAV2, AAV2g9 or AAV2i8g9 packaging the CBh-ScGFP transgene into the left lateral ventricle (ICV). One cohort of mice was coinjected with 1 μ g soluble heparin (Hep) per mouse as indicated. 2 weeks post vector administration, the mice were sacrificed and the brains were harvested and immunostained for comparing transgene (GFP) expression (black). (a–d) Representative images of hippocampal sections from AAV2, AAV2g9, AAV2g9+Heparin or AAV2i8g9 injections have been shown. (e) Higher magnification images of GFP expression (black) in different regions of the mouse brain namely; somatosensory cortex (SCT), piriform CT, motor CT, dentate gyrus (DG), amygdala (AMG) and hippocampal CA1, CA2 and CA3 regions have been shown. The Zeiss CLSM 700 confocal laser scanning microscope was used to image stitched images of entire mouse brain and higher magnification images of individual regions. All experiments were conducted in triplicate and representative images are shown. AAV, adeno-associated viral; GFP, green fluorescent protein; ICV, intracerebroventricular injections; cBh, chicken β actin hybrid.

with AAV9. Consistent with biodistribution data, AAV2g9 treated mice exhibit near background levels of GFP expression in both ICV and IT cohorts. Together, these results are also consistent with the reduced leakage of AAV2g9 vectors (>100-fold) into the blood circulation that was observed in comparison to AAV9 vectors (Figure 7). Briefly, AAV9 vector genomes were observed in blood as early as 15 minutes postadministration and continued to decline over 2 days. These results are consistent with earlier studies reported by our lab and others.^{32,33} In contrast, AAV2g9 vector genomes remained near background levels with a slight increase in copy number observed at the 24- and 48-hour time intervals. Together, our results confirm that unlike AAV9, AAV2g9 undergoes significantly reduced systemic leakage following CNS administration and consequently displays low levels of sequestration and transgene expression in peripheral organs.

Brain-restricted deletion of MIR137 gene using AAV2g9 in CRISPR-Cas9 knock-in mice

We have established that CNS administration of AAV2g9 results in limited systemic exposure and efficient gene transfer within the neural tissue. To further validate the potential advantages of the latter attributes, we generated AAV2g9 vectors packaging two guide RNAs (gRNAs) for targeted disruption of the *MIR137* gene in the brain. Specifically, the gRNAs were designed to recognize both ends of the 85bp pre-MIR137 region. Equal doses of AAV2g9 packaging MIR137gRNA or controlgRNA were administered into Cas9

transgenic mice⁹ via unilateral ICV injections. At 2 weeks post vector administration the mice were sacrificed and organs were harvested. Brain and liver tissues were then subject to genomic DNA extraction. To evaluate gene disruption events, we utilized the droplet digital PCR (ddPCR) technique. Briefly, primers were designed to amplify 206bp mouse genomic regions flanking the MIR137 target locus. Fluorescent probes were designed to bind MIR137gRNA target region (FAM, red) and an unspecific downstream locus (HEX, green). Successful disruption of MIR137 locus results in exclusive excitation of HEX probe alone (green), whereas both FAM and HEX probes are excited (orange) in case of no gene disruption events (Figure 8a). Next, ddPCR analysis revealed that the frequency of MIR137 eliminated alleles was significantly higher (green dots) in mice that received AAV2g9-MIR137gRNA, as compared with AAV2g9-controlgRNA cohort (Figure 8c, red arrow). Correspondingly, quantitative analysis of this phenomenon demonstrated a significant increase in mutant allele frequency within the MIR137gRNA injected mouse brains (Figure 8d).

Next, we examined whether AAV2g9 vector-mediated gene disruption events were specific to the brain. Identical ddPCR analysis conducted on liver DNA extracted from the same mouse cohorts displayed near background levels of MIR137 elimination in the systemic organ (Figure 8e). Further quantitation demonstrated negligible mutant allele formation due to both AAV2g9-controlgRNA and AAV2g9-MIR137gRNA injections in the liver (Figure 8f). In addition, consistent with

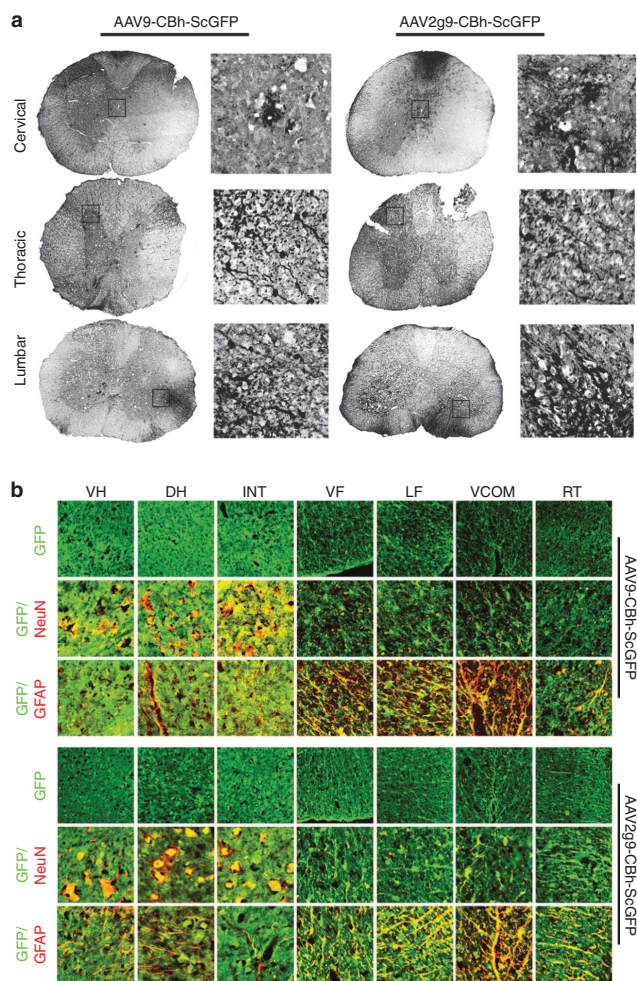


Figure 5 Comparison of transgene (GFP) expression and cellular tropism displayed by AAV9 and AAV2g9 vectors following intrathecal (IT) infusion. (a) Spinal cord sections showing cervical, thoracic and lumbar regions obtained from 8 week old adult C57/BL6 male mice infused with AAV9 or AAV2g9 packaging the CBh-ScGFP transgene (1×10^{11} vg) by lumbar puncture. Mice were sacrificed and the spinal cords were postfixed in paraformaldehyde, sectioned at 3 weeks post vector administration. Diaminobenzidine (DAB) immunohistochemistry was used to detect GFP expression. Inset images from whole spinal cord cross-sections are shown to the right of each section at higher magnification. **(b)** Representative confocal images of immunostained sections at higher magnification. GFP expression (top panel, green) in the ventral horn (VH), dorsal horn (DH), intermediate zone gray matter (INT), ventral funiculus (VF), lateral funiculus (LF), ventral commissure (VC) and rubrospinal tract (RT) regions is shown. Middle and bottom panels show immuno-colocalization of GFP expression (green) with neuronal marker, NeuN or glial marker, GFAP (red) obtained using a Zeiss CLSM 700 confocal laser scanning microscope equipped with 488, 555, and 647 nm excitation filters. Colocalized cells are pseudocolored yellow (GFP/NeuN or GFP/GFAP overlay). All experiments were conducted in triplicate and representative images are shown. AAV, adeno-associated viral; GFAP, glial fibrillary acid protein; GFP, green fluorescent protein; ICV, intracerebroventricular injections; cBh, chicken β actin hybrid.

earlier results, AAV2g9 vector genome biodistribution analysis demonstrated significant enrichment of AAV genomes within the brain in comparison with systemic liver tissue (Figure 8b). Overall, our data demonstrates CNS-restricted

gene disruption within the Cas9 transgenic mouse using ICV administration of engineered AAV2g9 vector.

Discussion

Recent large scale GWAS studies conducted across ~40,000 patients led to the discovery that disruption in *MIR137* gene function is strongly correlated with Schizophrenia disease occurrence.^{34,35} Here, we utilize this well-known gene target to illustrate the utility of a novel, lab-derived AAV vector for CNS-specific gene transfer. Since *MIR137* and CAG promoter driven Cas9 are both expressed constitutively in brain and liver tissue,^{9,36} it is safe to assume that brain specific *MIR137* disruption relies on AAV2g9 vector design. The efficiency of AAV-mediated gene editing achieved in the current study is similar to that demonstrated earlier with the CRISPR/Cas9 knock-in mouse model.⁹ However, improvements to vector design could further improve gene editing efficiency. More importantly, from the vector development perspective, these studies have broad implications for gene therapy, silencing and editing.

First, it should be noted that the CNS transduction efficiency and systemic gene expression from a single ICV/IT dose of AAV9 is striking. Although this might not be ideal for certain CNS-specific indications due to the systemic leakage profile, AAV9 is certainly an optimal vector candidate for treatment of lysosomal storage disorders and other such diseases, which are characterized by multiorgan involvement in addition to the CNS. On the other hand, AAV2g9 displays favorable attributes for therapeutic applications targeting neuronal populations within the CNS. Further, the features displayed by the engineered AAV2g9 strain exemplify the feasibility of making rational improvements to AAV vector design with the goal of imparting favorable biodistribution profiles. When combined with cell-specific elements such as the hSyn promoter, as established in the current study or miRNA targeting elements,^{22,23} such approaches could help restrict transgene expression to neuronal populations within the CNS and reduce systemic exposure. In addition, therapeutic delivery of gene editing nucleases using AAV2g9 could help mitigate the risk for off-target effects at the organ level.

From the AAV biology perspective, these studies provide new insights into the role of capsid-glycan interactions in determining CNS spread and systemic leakage. Earlier studies in our lab and others have demonstrated that the diverse cellular tropisms and biodistribution profiles of different AAV strains is intricately linked to their glycan receptor binding profiles.^{37,38} For instance, intracranial injection of the HS binding strain, AAV2 shows restricted, neuronal gene expression.²⁷ This preferential neuronal tropism of AAV2 appears to correlate with the higher concentration of heparan sulfate proteoglycans on the surface of neurons compared with glia.³⁹ Accordingly, AAV2g9 retains its preferential neuronal tropism, likely due to its ability to bind HS within the CNS. Correspondingly, both competitive inhibition with soluble heparin coadministration and disrupting HS binding with loss of function capsid mutation (AAV2i8g9) resulted in ablated neuronal transduction *in vivo*. However, as a caveat to this neurotropic bias, the ability of AAV2 to bind HS with

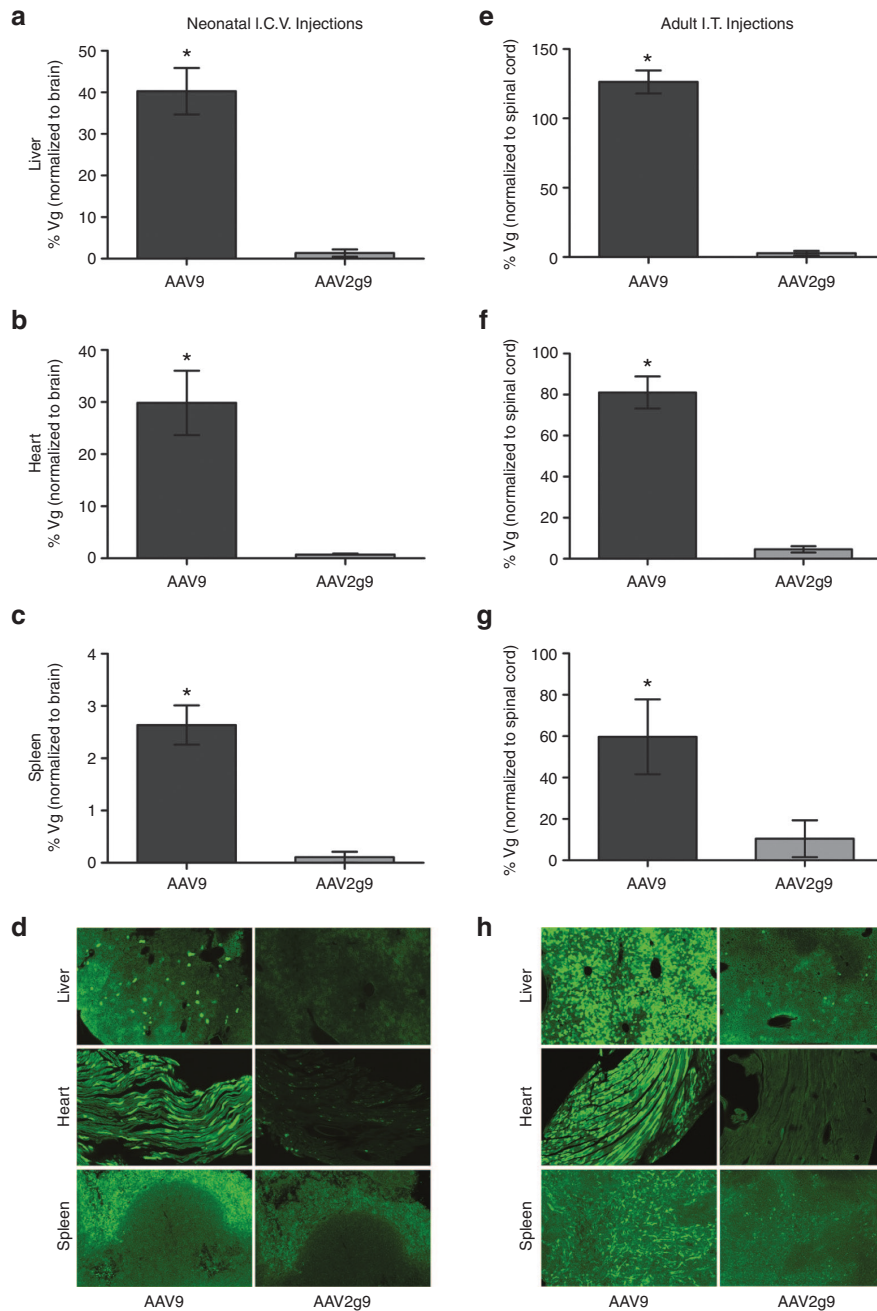


Figure 6 Comparison of systemic biodistribution and off-target transgene (GFP) expression displayed by ICV/IT injected AAV9 and AAV2g9 vectors. (a–c) Relative percentage of vector genome (vg) copy numbers for AAV9 (dark gray bars) and AAV2g9 (light gray bars) in systemic organs, *i.e.*, liver, heart, and spleen normalized to vg copy number in the brain following ICV administration in neonates. (d) Confocal micrographs showing GFP expression in systemic organs – liver, heart, and spleen obtained from neonatal ICV cohorts. (e–g) Relative percentage of vg copy numbers for AAV9 (dark gray bars) and AAV2g9 (light gray bars) in systemic organs, *i.e.*, liver, heart, and spleen normalized to vg copy number in the spinal cord following IT administration in adult mice. (h) Confocal micrographs showing GFP expression in systemic organs – liver, heart, and spleen obtained from adult IT cohorts. The vg copy per host genome (vg/cell) was determined by quantitative polymerase chain reaction (PCR) of extracted DNA and normalized to the number of copies of the mouse lamin $\beta 2$ gene. Data shown is represented as mean \pm SD; Statistical significance ($*P < 0.05$) was established using student's *t*-test. All experiments were conducted in quadruplicate and representative images are shown. AAV, adeno-associated viral; GFP, green fluorescent protein; ICV, intracerebroventricular injections; IT, intrathecal.

high affinity also restricts vector spread and the effective volume of CNS tissue transduced.²⁸ In contrast, the galactose binding strain, AAV9, shows both neuronal and glial transduction as well as efficient CNS spread.^{18,40} One possible

explanation for the increased spread of AAV2g9 as compared with AAV2 can be attributed to capsid interactions with proteins in the CSF that might facilitate spread and transport within the brain. Alternatively, while axonal transport of AAV2

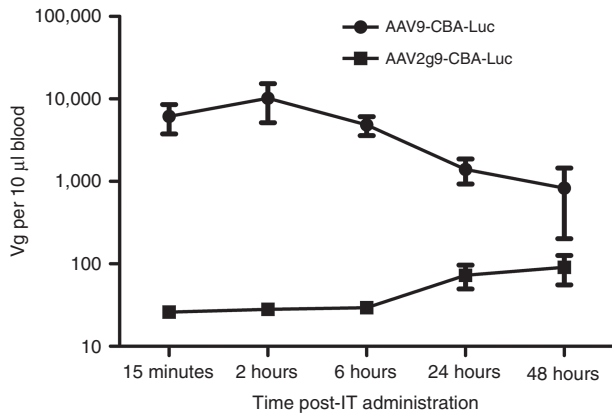


Figure 7 Comparison of blood circulation/pharmacokinetic profiles AAV9 and AAV2g9 vectors in adult mice post intrathecal (IT) administration. A 8 week old Balb/C mice were injected with equal viral titers (7.8×10^9 vg) of AAV9 or AAV2g9 packaging CBA-Luc transgene via IT injections. Approximately 10 μ l blood was collected via tail vein nicks from adult mice at 15 minutes, 2 hours, 6 hours, 24 hours, and 48 hours post IT injection. Blood samples were immediately mixed with equal volume of sodium citrate (3.8% weight/volume) to avoid coagulation. Pharmacokinetic profiles of AAV9/2g9 vectors were generated using quantitative polymerase chain reaction (qPCR) to calculate viral genomes in the blood samples with primers specific to the luciferase transgene. Data represents mean \pm SEM. * represents $P < 0.05$ as determined by student's *t*-test. All experiments were conducted in quadruplicate. AAV, adeno-associated viral; CBA, chicken β actin.

is exclusively restricted to the anterograde direction, AAV9 is known to travel in both anterograde and retrograde directions to cover long distances within the neural tissue.^{16,21,37,40} We acknowledge that such hypotheses warrant further evaluation and such detailed studies will likely shed light on the mechanism(s) driving enhanced CNS spread of the dual glycan binding AAV2g9. Consistent with the latter attributes, AAV9 capsids also appear to be prone to systemic leakage and transduction in the liver and other organs following CNS administration.^{19,22,23} In this study, the dual glycan binding strain has inherited traits from both parental AAV serotypes, *i.e.*, neurotropism from AAV2 and robust CNS spread and transduction from AAV9.

Materials and methods

Recombinant AAV vector production. An updated triple plasmid transfection protocol was used to generate recombinant AAV vectors. The pXR2g9 and pXR2i8g9 plasmids have been described earlier.²⁶ All other plasmids used for AAV production in this study were obtained from the UNC vector core. Briefly, the transfection mixture contained (i) the pXR9 helper plasmid or pXR2g9/2i8g9 helper plasmids; (ii) the adenoviral helper plasmid pXX6-80; and (iii) pTR-CBh-ScGFP, pTR-hSyn-EGFP, pTR-GFAP-EGFP or pTR-CBA-Luc plasmids encoding the GFP or luciferase (Luc) reporter genes driven by the CBh, hSyn, GFAP or the chicken β actin (CBA) promoters, flanked by inverted terminal repeats derived from the AAV2 genome. Vector purification was carried out using iodaxinol gradient ultracentrifugation protocol, buffer exchange and concentration using vivaspin2 100 kDa molecular weight

cut-off (MWCO) centrifugation columns (F-2731-100 Bioexpress, Kaysville, UT). Vg titers were obtained by quantitative PCR (Lightcycler 480, Roche Applied Sciences, Pleasanton, CA) using primers designed to selectively bind AAV2 inverted terminal repeats (forward, 5'- AAC ATG CTA CGC AGA GAG GGA GTG G-3'; reverse, 5'- CAT GAG ACA AGG AAC CCC TAG TGA TGG AG-3') (IDT Technologies, Ames, IA).

ICV administration. Animal experiments reported in this study were conducted with Balb/C or C57/Bl6 mice bred and maintained in accordance to NIH guideline as approved by the UNC Institutional Animal Care and Use Committee (IACUC). Postnatal day 0 (P0) Balb/c pups which were rapidly anesthetized on ice for 2 minutes followed by stereotaxic ICV injections. Specifically, AAV9 or AAV2g9 vectors packaging different transgenes were injected into the left lateral ventricle (total volume < 3 μ l) using a Hamilton 700 series syringe with a 26s gauge needle (Sigma-Aldrich, St. Louis, MO), attached to a KOPF-900 small animal stereotaxic instrument (KOPF instruments, Tujunga, CA). All neonatal injections were performed 0.5mm relative to the sagittal sinus, 2mm rostral to transverse sinus and 1.5mm deep. Following vector administration, mice were revived under a heat lamp and rubbed in the bedding before being placed back with the dam. At 2 weeks post vector administrations (P14) the mouse brains were harvested, postfixed and immunostained as described below in detail. For coadministration of soluble heparin (generously provided by Dr Jian Liu, School of Pharmacy, UNC), AAV vectors (3.5×10^9 vg) were mixed with 1 μ g of heparin and a total volume of 2–3 μ l administered per mouse for 30 minutes on ice prior to ICV injections in neonatal mice.

IT administration. AAV vectors were infused into the mouse IT cerebrospinal fluid space using Alzet mouse IT catheter and pump (Alzet, 0007743, Durect, Cupertino, CA). Briefly, the pumps were primed with 0.9% NaCl for ~12 hours followed by AAV vectors. Later 8 weeks old C57/Bl6 males were anesthetized with intraperitoneal injection of Avertin (1.25%, 2,2,2-tribromoethanol in phosphate-buffered saline) at 0.23 ml/10g body weight prior to infusions. A 23 gauge needle was used to expose the L5–L6 intervertebral space and the osmotic pump was implanted and sutured under the skin. The vector was then infused at the rate of ~8 μ l/hr for ~24 hours to infuse a total 1×10^{11} vg of AAV9 and AAV2g9 vectors packaging the CBh-ScGFP transgene. At 3 weeks post administration of the vectors, the mice were sacrificed, postfixed in paraformaldehyde, sectioned and immunostained as described below. Another cohort of 8 week old Balb/C mice was injected via IT bolus injections with AAV9 and AAV2g9 vectors as described elsewhere.⁴¹ Briefly, equal titers of vectors packaging the CBA-Luc transgene cassette (total volume 4–5 μ l) was free-hand injected into the L5 and L6 intervertebral space. The injections were carried out an angle of 20–30 degrees from spinal column using the 30G disposable needle attached to 50 μ l Luer-hub Hamilton syringe (Sigma-Aldrich).

Vector genome biodistribution and pharmacokinetic analyses. Cohorts of neonatal and adult mice used for biodistribution studies were sacrificed 3 days post vector administration via the ICV or IT bolus routes. The genomic DNA was extracted

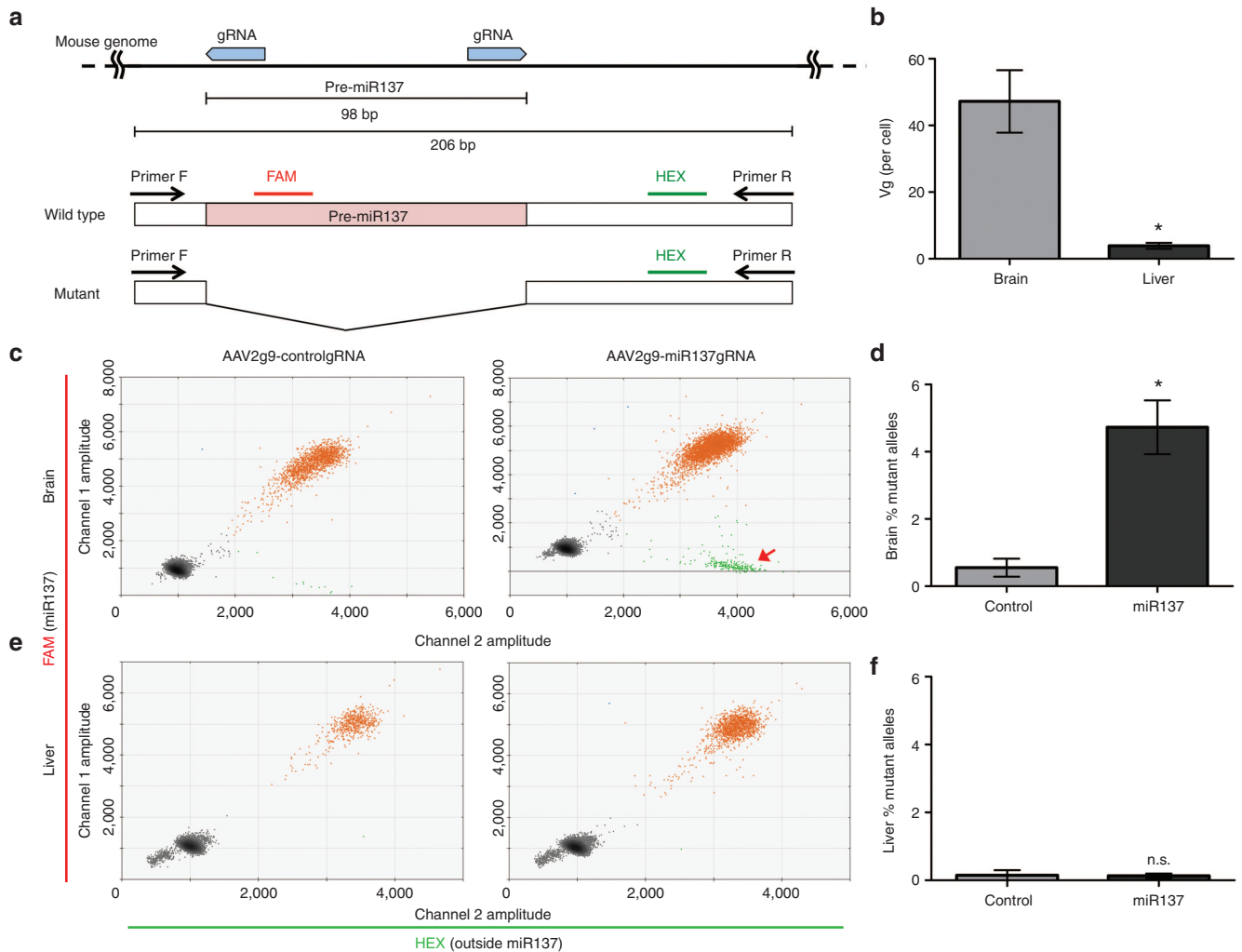


Figure 8 CNS-restricted gene disruption of MIR137 within Cas9 transgenic mouse using AAV2g9. (a) Schematic representation of mouse MIR137 locus (mm10, chr3:118, 433, 800-118, 434, 004). Two gRNAs were designed to generate a 98 bp deletion within pre-MIR137 region. Droplet digital PCR (ddPCR) primers were designed to amplify a 206 bp region (wild type mir-137) and shorter mutant (mir-137 eliminated) genomic DNA. Probes were designed to detect (i) unaltered region (HEX probe, green) and (ii) a region flanked by two MIR137gRNAs (FAM probe, red). (b) AAV2g9 vector genome (vg) copy numbers (per cell) within the brain (light gray bars) and liver (dark gray bars) tissues, 2 weeks post ICV administration in neonatal (P0) Cas9 transgenic mice. Scatter plots showing results of ddPCR on brain (c) and liver (e) genomic DNA from AAV2g9-controlgRNA (left) or AAV2g9-MIR137gRNA (right) injected mice. Specifically, HEX+/FAM+ double positive droplets (Orange) indicate wildtype alleles, while HEX+/FAM- droplets (Green; depicted by red arrow) demonstrate MIR137 eliminated alleles. Results from all samples ($n = 3$ or 4) are pooled to generate these plots. (d and f) Quantitative analyses of ddPCR from controlgRNA (light gray bars) and MIR137gRNA (dark gray bars). Wild-type and mutant allele were predicted using a 2D dot plot as shown. Because the number of droplets with a fluorescent signal is low (<5%), we can assume that most of the positive droplets have one allele.⁴³ Graphical data represents mean \pm SEM. *represents $P < 0.05$, n.s. indicates 'not statistically significant' ($P > 0.05$), as determined by student's t -test. All experiments were conducted in triplicate. AAV, adeno-associated viral; CNS, central nervous system; ICV, intracerebroventricular injections. Reprinted from ref. 43.

from the tissue lysates and blood using the DNeasy kit (Qiagen, Valencia, CA). To calculate viral genome copy numbers quantitative polymerase chain reaction was performed with primers specific to luciferase transgene 5'-AAAAGCACTCTGATTGACAAATAC-3' and 5'-CCTTCGCTTCAAAAAATGGAA C-3'. The vector genome copy numbers were normalized to mouse lamin B2 locus as the housekeeping gene using the primers 5'-GGACCAAGGACTACCTCAAGGG-3' and 5'-AGGGCACCTCCATCTCGGAAAC-3'. The vector biodistribution was represented as the ratio of vector genomes per cell recovered in the peripheral organs to the CNS site of

injection (brain or the spinal cord). For pharmacokinetic studies, the vector genome copy numbers were calculated from total DNA isolated from 10 μ l blood.

Tissue processing, immunofluorescence, and confocal microscopy. Neonatal and adult mouse cohorts were sacrificed 2 weeks and 3 weeks post vector administrations respectively. The mice were overdosed with tribromoethanol (avertin) (0.2 ml/10 g of 1.25% solution) via the intraperitoneal route. This was followed by transcardial perfusions of phosphate-buffered saline and 4% paraformaldehyde in

phosphate-buffered saline. The organs were removed and postfixed for 24 hour prior to sectioning. Briefly, 50 μ m thick sections were obtained using a Leica VT 1,200S vibrating blade microtome (Leica Biosystems, Buffalo Grove, IL). The spinal cords were cryo-sectioned by UNC animal histopathology core. The sections of mouse organs from various treatments were blocked in 10% goat serum (Sigma-Aldrich) and 1% Triton X (Sigma-Aldrich) in phosphate-buffered saline for 1 hour. This was followed by overnight incubation with primary monoclonal antibodies at 4°C. The primary antibodies utilized as a part of this study are as follows: Rabbit anti-GFP (Life-Technologies-G10,362, 1:750) mouse anti-GFAP (Abcam-10,062, 1:1,000), rabbit anti-NeuN (Abcam-104,225, 1:750), chicken anti-GFP (Abcam-13,970, 1:750). Secondary antibodies were raised in goats and conjugated to Alexa 488 (anti-rabbit Abcam-96,883, anti-chicken Abcam-96,947), Alexa 594 (anti-Rabbit Abcam-96,885) or Alexa 647 (anti-mouse Abcam-150,115). The secondary antibodies were used at a standard dilution of 1:500. The immunohistochemical analyses of GFP expression was conducted using Vectastain ABC kit (Rabbit IgG PK-4001 kit, Vector bio-labs, Burlingame, CA). We used Zeiss CLSM 700 confocal laser scanning microscope for imaging sections of different organs after immunostaining (Microscopy Services Laboratory, UNC). The images were stitched, pseudocolored, and analyzed on the Zen Black v 10.0 software.

CRISPR gRNA design. Two gRNAs were designed to detect 98bp Pre-MIR137 flanking region and analyzed by COSMID (crispr.bme.gatech.edu) to check potential off-target sites.⁴² Target sequencing used to make the gRNAs are following: mir-137-g1;CGTCACCGAAGAGAGTCAG, mir-137-g3;GTAGTCGAGGAGAGTACCAG. For control gRNA, we used a 20bp sequence, which recognizes an unspecific backbone region of plasmid DNA (Con-g1; GTCGACTCTAGAGGATCCAC). Tandem repeat of U6 promoter-target sequence-guideRNA is conjugated with EF1core promoter-tdTomato-P2A-PuroR and subcloned into the pTR vector for packaging into AAV.

Droplet digital PCR. PureLink Genomic DNA extraction kit (Thermo Fisher Scientific, K182,002) was used to obtain DNA from brain and liver tissues. Following sequences of primers and probes were used for the ddPCR assay. MMIR137L206ddPCR; GCAGCAGTGACAGCGGTAGC, MMIR137R206ddPCR; TGGCAACCGGGAGCTTTTAG, MMIR137MTFAMddPCR; /56-FAM/TCCACCCAA/ZEN/GAATACCCGTCACCG/3IABkFQ/, MMIR137WTHExddPCR; /5HEX/CCCTCCAG/ZEN/CCCACAGCTG/3IABkFQ/.

For ddPCR, 2x ddPCR Supermix for Probes (No dUTP; Bio-rad, 1,863,023), the QX100 Droplet generator and reader (Bio-rad) were employed. 10ng genomic DNAs were subjected to PCR amplification by C1,000 thermal cycler (Bio-rad) with the following condition: 95°C 10 minutes x 1, (4°C 30 seconds, 65°C 1 minutes) x40, 98°C 10 minutes x1; 2°C/sec. Obtained data was analyzed by the QuantaSoft software (Bio-rad).

Study approval. All neonatal and adult Balb/c or C57/Bl6 mice used in the study were bred, maintained and utilized in accordance to NIH guidelines as approved by the UNC

Institutional Animal Care and Use Committee (IACUC) (Protocol # 15–109).

Acknowledgments We would like to acknowledge NIH for research funding awarded to A.A. (R01HL089221 and P01HL112761); G.G. (R01NS076991); and P.S. (R21MH102814). We would like to disclose that Aravind Asokan (corresponding author) is a cofounder at Stridebio, LLC and an inventor on patents owned by UNC-Chapel Hill; Guangping Gao (coauthor) is an inventor on several patents and a scientific founder of Voyager Therapeutics.

Author contributions G.M. and A.A. conceived the study. G.M., L.R., and T.C. carried out vector production, administration, histology, and image analysis. K.S. and P.S. conducted the gRNA design and gene disruption analyses. D.W. and G.G. assisted with IT administration and provided input for the overall study. G.M. and A.A. analyzed the data and wrote the manuscript.

1. Flotte, TR (2013). Birth of a new therapeutic platform: 47 years of adeno-associated virus biology from virus discovery to licensed gene therapy. *Mol Ther* **21**: 1976–1981.
2. Nathwani, AC, Reiss, UM, Tuddenham, EG, Rosales, C, Chowdhury, P, McIntosh, J *et al.* (2014). Long-term safety and efficacy of factor IX gene therapy in hemophilia B. *N Engl J Med* **371**: 1994–2004.
3. Tuszynski, MH, Yang, JH, Barba, D, U, HS, Bakay, RA, Pay, MM *et al.* (2015). Nerve growth factor gene therapy: activation of neuronal responses in Alzheimer disease. *JAMA Neurol* **72**: 1139–1147.
4. Jacobson, SG, Cideciyan, AV, Roman, AJ, Sumaroka, A, Schwartz, SB, Heon, E *et al.* (2015). Improvement and decline in vision with gene therapy in childhood blindness. *N Engl J Med* **372**: 1920–1926.
5. Mingozi, F and High, KA (2013). Immune responses to AAV vectors: overcoming barriers to successful gene therapy. *Blood* **122**: 23–36.
6. Gao, K, Li, M, Zhong, L, Su, Q, Li, J, Li, S *et al.* (2014). Empty virions in AAV8 vector preparations reduce transduction efficiency and may cause total viral particle dose-limiting side-effects. *Mol Ther Methods Clin Dev* **1**: 20139.
7. Yin, H, Song, CQ, Dorkin, JR, Zhu, LJ, Li, Y, Wu, Q *et al.* (2016). Therapeutic genome editing by combined viral and nonviral delivery of CRISPR system components *in vivo*. *Nat Biotechnol* **34**: 328–333.
8. Swiech, L, Heidenreich, M, Banerjee, A, Habib, N, Li, Y, Trombetta, J *et al.* (2015). *In vivo* interrogation of gene function in the mammalian brain using CRISPR-Cas9. *Nat Biotechnol* **33**: 102–106.
9. Platt, RJ, Chen, S, Zhou, Y, Yim, MJ, Swiech, L, Kempton, HR *et al.* (2014). CRISPR-Cas9 knockin mice for genome editing and cancer modeling. *Cell* **159**: 440–455.
10. Ran, FA, Cong, L, Yan, WX, Scott, DA, Gootenberg, JS, Kriz, AJ *et al.* (2015). *In vivo* genome editing using Staphylococcus aureus Cas9. *Nature* **520**: 186–191.
11. Nelson, CE, Hakim, CH, Ousterout, DG, Thakore, PI, Moreb, EA, Castellanos Rivera, RM *et al.* (2016). *In vivo* genome editing improves muscle function in a mouse model of Duchenne muscular dystrophy. *Science* **351**: 403–407.
12. Tabeqborbar, M, Zhu, K, Cheng, JK, Chew, WL, Widrick, JJ, Yan, WX *et al.* (2016). *In vivo* gene editing in dystrophic mouse muscle and muscle stem cells. *Science* **351**: 407–411.
13. Gao, G, Alvira, MR, Somanathan, S, Lu, Y, Vandenbergh, LH, Rux, JJ *et al.* (2003). Adeno-associated viruses undergo substantial evolution in primates during natural infections. *Proc Natl Acad Sci USA* **100**: 6081–6086.
14. Gao, G, Vandenbergh, LH, Alvira, MR, Lu, Y, Calcedo, R, Zhou, X *et al.* (2004). Clades of adeno-associated viruses are widely disseminated in human tissues. *J Virol* **78**: 6381–6388.
15. Hastie, E and Samulski, RJ (2015). Adeno-associated virus at 50: a golden anniversary of discovery, research, and gene therapy success—a personal perspective. *Hum Gene Ther* **26**: 257–265.
16. Ojala, DS, Amara, DP and Schaffer, DV (2015). Adeno-associated virus vectors and neurological gene therapy. *Neuroscientist* **21**: 84–98.
17. Bartus, RT, Weinberg, MS and Samulski, RJ (2014). Parkinson's disease gene therapy: success by design meets failure by efficacy. *Mol Ther* **22**: 487–497.
18. Foust, KD, Nurre, E, Montgomery, CL, Hernandez, A, Chan, CM and Kaspar, BK (2009). Intravascular AAV9 preferentially targets neonatal neurons and adult astrocytes. *Nat Biotechnol* **27**: 59–65.
19. Gray, SJ, Matagne, V, Bachaboina, L, Yadav, S, Ojeda, SR and Samulski, RJ (2011). Preclinical differences of intravascular AAV9 delivery to neurons and glia: a comparative study of adult mice and nonhuman primates. *Mol Ther* **19**: 1058–1069.
20. Bevan, AK, Duque, S, Foust, KD, Morales, PR, Braun, L, Schmelzer, L *et al.* (2011). Systemic gene delivery in large species for targeting spinal cord, brain, and peripheral tissues for pediatric disorders. *Mol Ther* **19**: 1971–1980.

21. Samaranch, L, Salegio, EA, San Sebastian, W, Kells, AP, Foust, KD, Bringas, JR *et al.* (2012). Adeno-associated virus serotype 9 transduction in the central nervous system of nonhuman primates. *Hum Gene Ther* **23**: 382–389.
22. Yang, B, Li, S, Wang, H, Guo, Y, Gessler, DJ, Cao, C *et al.* (2014). Global CNS transduction of adult mice by intravenously delivered rAAVrh.8 and rAAVrh.10 and nonhuman primates by rAAVrh.10. *Mol Ther* **22**: 1299–1309.
23. Xie, J, Xie, Q, Zhang, H, Ameres, SL, Hung, JH, Su, Q *et al.* (2011). MicroRNA-regulated, systemically delivered rAAV9: a step closer to CNS-restricted transgene expression. *Mol Ther* **19**: 526–535.
24. Rosenberg, JB, Sondhi, D, Rubin, DG, Monette, S, Chen, A, Cram, S *et al.* (2014). Comparative efficacy and safety of multiple routes of direct CNS administration of adeno-associated virus gene transfer vector serotype rh.10 expressing the human arylsulfatase: a cDNA to nonhuman primates. *Hum Gene Ther Clin Dev* **25**: 164–177.
25. Shen, S, Bryant, KD, Brown, SM, Randell, SH and Asokan, A (2011). Terminal N-linked galactose is the primary receptor for adeno-associated virus 9. *J Biol Chem* **286**: 13532–13540.
26. Shen, S, Horowitz, ED, Troupes, AN, Brown, SM, Pulicherla, N, Samulski, RJ *et al.* (2013). Engraftment of a galactose receptor footprint onto adeno-associated viral capsids improves transduction efficiency. *J Biol Chem* **288**: 28814–28823.
27. Davidson, BL, Stein, CS, Heth, JA, Martins, I, Kotin, RM, Derksen, TA *et al.* (2000). Recombinant adeno-associated virus type 2, 4, and 5 vectors: transduction of variant cell types and regions in the mammalian central nervous system. *Proc Natl Acad Sci USA* **97**: 3428–3432.
28. Burger, C, Gorbatyuk, OS, Velardo, MJ, Peden, CS, Williams, P, Zolotukhin, S *et al.* (2004). Recombinant AAV viral vectors pseudotyped with viral capsids from serotypes 1, 2, and 5 display differential efficiency and cell tropism after delivery to different regions of the central nervous system. *Mol Ther* **10**: 302–317.
29. Summerford, C and Samulski, RJ (1998). Membrane-associated heparan sulfate proteoglycan is a receptor for adeno-associated virus type 2 virions. *J Virol* **72**: 1438–1445.
30. Nguyen, JB, Sanchez-Pernaute, R, Cunningham, J and Bankiewicz, KS (2001). Convection-enhanced delivery of AAV-2 combined with heparin increases TK gene transfer in the rat brain. *Neuroreport* **12**: 1961–1964.
31. Mastakov, MY, Baer, K, Kotin, RM and During, MJ (2002). Recombinant adeno-associated virus serotypes 2- and 5-mediated gene transfer in the mammalian brain: quantitative analysis of heparin co-infusion. *Mol Ther* **5**: 371–380.
32. Kotchey, NM, Adachi, K, Zahid, M, Inagaki, K, Charan, R, Parker, RS *et al.* (2011). A potential role of distinctively delayed blood clearance of recombinant adeno-associated virus serotype 9 in robust cardiac transduction. *Mol Ther* **19**: 1079–1089.
33. Shen, S, Bryant, KD, Sun, J, Brown, SM, Troupes, A, Pulicherla, N *et al.* (2012). Glycan binding avidity determines the systemic fate of adeno-associated virus type 9. *J Virol* **86**: 10408–10417.
34. Schizophrenia Psychiatric Genome-Wide Association Study (GWAS) Consortium (2011). Genome-wide association study identifies five new schizophrenia loci. *Nat. Genet.* **43**: 969–976.
35. Kwon, E, Wang, W and Tsai, LH (2013). Validation of schizophrenia-associated genes CSMD1, C10orf26, CACNA1C and TCF4 as miR-137 targets. *Mol Psychiatry* **18**: 11–12.
36. Chen, S, He, N, Yu, J, Li, L, Hu, Y, Deng, R *et al.* (2014). Post-transcriptional regulation by miR-137 underlies the low abundance of CAR and low rate of bilirubin clearance in neonatal mice. *Life Sci* **107**: 8–13.
37. Murlidharan, G, Samulski, RJ and Asokan, A (2014). Biology of adeno-associated viral vectors in the central nervous system. *Front Mol Neurosci* **7**: 76.
38. Bell, CL, Vandenberghe, LH, Bell, P, Limberis, MP, Gao, GP, Van Vliet, K *et al.* (2011). The AAV9 receptor and its modification to improve *in vivo* lung gene transfer in mice. *J Clin Invest* **121**: 2427–2435.
39. Hsueh, YP and Sheng, M (1999). Regulated expression and subcellular localization of syndecan heparan sulfate proteoglycans and the syndecan-binding protein CASK/LIN-2 during rat brain development. *J Neurosci* **19**: 7415–7425.
40. Cearley, CN and Wolfe, JH (2007). A single injection of an adeno-associated virus vector into nuclei with divergent connections results in widespread vector distribution in the brain and global correction of a neurogenetic disease. *J Neurosci* **27**: 9928–9940.
41. Fairbanks, CA (2003). Spinal delivery of analgesics in experimental models of pain and analgesia. *Adv Drug Deliv Rev* **55**: 1007–1041.
42. Cradick, TJ, Qiu, P, Lee, CM, Fine, EJ and Bao, G (2014). COSMID: A Web-based tool for identifying and validating CRISPR/Cas off-target sites. *Mol Ther Nucleic Acids* **3**: e214.
43. Hindson, BJ, Ness, KD, Masquelier, DA, Belgrader, P, Heredia, NJ, Makarewicz, AJ *et al.* (2011). High-throughput droplet digital PCR system for absolute quantitation of DNA copy number. *Anal Chem* **83**: 8604–8610.



This work is licensed under a Creative Commons Attribution-NonCommercial-ShareAlike 4.0 International License. The images or other third party material in this article are included in the article's Creative Commons license, unless indicated otherwise in the credit line; if the material is not included under the Creative Commons license, users will need to obtain permission from the license holder to reproduce the material. To view a copy of this license, visit <http://creativecommons.org/licenses/by-nc-sa/4.0/>

© G Murlidharan *et al.* (2016)